Journal of Fluids and Structures (2002) **16**(6), 739–759
doi:10.1006/jfls.445 available online at http://www.idealibrary.com on IDEAL®

LINEAR AND NONLINEAR DYNAMICS OF CANTILEVERED CYLINDERS IN AXIAL FLOW. PART 3: NONLINEAR DYNAMICS

C. Semler, J. L. Lopes†, N. Augu‡ and M.P. Païdoussis

Department of Mechanical Engineering, McGill University, 817 Sherbroke Street West Montreal, Québec, Canada H3A 2K6

(Received 25 January 2001; and in final form 27 November 2001)

The dynamics of a cantilevered cylinder in axial flow are explored, by means of the equations derived in Part 2 of this three-part study, and using as numerical tools the finite difference method and AUTO in order to solve the discretized equations. The linear dynamics is considered first, focusing on the effect of some key parameters on stability. Then, the nonlinear dynamics is examined by means of concrete examples with parameters close to those in the experiments of Part 1, by means of bifurcation diagrams, phase-plane plots and Poincaré maps. The agreement between theory and experiment is qualitatively good and quantitatively reasonable, in terms of the critical values for the various bifurcations, and the amplitudes and frequencies of the motions observed.

1. INTRODUCTION

The main purpose of this three-part paper is the re-examination of the linear dynamics of a cantilevered cylinder in axial flow and the exploration of some aspects of its nonlinear dynamics, as well as the comparison of both to experiments, some old, some new.

The experimental results are presented in Part 1 (Païdoussis *et al*. 2002), and comparison with linear theory is partly made therein, for convenience. The equations of motion are derived in Part 2 (Lopes *et al*. 2002). Here, the bulk of the theoretical results are presented, both linear and nonlinear, in Sections 3 and 4, respectively, followed by a comparison of theory and experiments. In Section 4, the comparison of the thresholds of instability, partly discussed in Part 1, is revisited, while comparison of distinctly nonlinear features of the dynamics is done in this paper for the first time. Some introductory comments follow, immediately below.

With the use of the model derived by Lopes *et al*. (2002), it is possible to study the dynamics of the system from a nonlinear point of view. Indeed, with the nonlinear equations, it is possible to find not only the different points of instability—the bifurcation points—but also to determine the dynamical response beyond these points.

†Presently at EADS Launch Vehicles, Les Mureaux Center Directorate, B.P. 3002, 66 Route de Verneuil, 78133 Les Mureaux Cedex, France.
‡Presently at Lore, filiale du groupe ALTRAN, 104 avenue du Président Kennedy, 75116 Paris, France.

0889-9746/02/060739 + 21 $35.00/0

Traditionally, for linear theory, i.e., using only the linear equations of motion, two types of bifurcation may occur: "divergence" and "flutter". Divergence corresponds to a static loss of stability, and might be associated with a pitchfork bifurcation. Physically, the cylinder loses its straight, undeformed configuration and it buckles as a column under axial load. Divergence, being a static instability, is associated with zero frequency; such a zero-frequency bifurcation could clearly also represent a static restabilization of the system and a return to the trivial, undeformed configuration of the cylinder. Flutter, on the other hand, represents a dynamic loss of stability, and is usually associated with a Hopf bifurcation. The cylinder thereafter develops amplified oscillation of finite frequency—a limit cycle.

Also possible by means of nonlinear theory is the prediction of divergence amplitudes and limit-cycle amplitude and frequency, and how these vary with flow, and many other quantitative post-bifurcation facets of dynamical behaviour.

2. THE ANALYTICAL MODEL

The equation of motion and boundary conditions have been derived by Lopes *et al.* (2002). Using Galerkin's method and the eigenfunctions $\phi_j(\xi)$ of a cantilever beam, they have been reduced to a set of ordinary differential equations that take the following form:

$$M_{ij}\ddot{q}_j + C_{ij}\dot{q}_j + K_{ij}q_j + r_{ijk}q_j|q_k| + \bar{s}_{ijk}|q_j|\dot{q}_k + \tilde{s}_{ijk}q_j|\dot{q}_k| + t_{ijk}\dot{q}_j|\dot{q}_k| + \alpha_{ijkl}q_jq_kq_l + \beta_{ijkl}q_jq_k\dot{q}_l + \gamma_{ijkl}q_j\dot{q}_k\dot{q}_l + \eta_{ijkl}\dot{q}_j\dot{q}_k\dot{q}_l + \mu_{ijkl}q_jq_k\ddot{q}_l = 0. \quad (1)$$

The indices i and j are integers ranging from 1 to N, where N represents the number of comparison functions. The terms M_{ij}, C_{ij}, K_{ij} correspond to the (linear) mass, damping and stiffness matrices, while α_{ijkl}, β_{ijkl}, γ_{ijkl}, η_{ijkl}, μ_{ijkl}, r_{ijk}, $\bar{s}_{ijk}$, $\tilde{s}_{ijk}$, and t_{ijk} are related to the nonlinear terms. They all depend on the different physical parameters, so the main task is to solve equation (1) numerically as a function of the main system parameters, which are introduced next.

2.1. Physical Parameters

For purposes of comparison with experiments, and in order to validate the theoretical model, physical parameters corresponding to one particular system have been used as much as possible. However, in order to give the theoretical work a broader spectrum and to enable us to draw more general conclusions, some additional values have been considered as well. The experiments have been fully described in Part 1 (Païdoussis *et al.* 2002) and have been conducted in a vertical water tunnel, using elastomer cylinders with a rigid tapering end. The major physical parameters are as follows:

$$D = 2{\cdot}54 \times 10^{-2}\,\mathrm{m}, \quad L = 0{\cdot}520\,\mathrm{m}, \quad \rho_c = 1\,150\,\mathrm{kg/m^3}, \quad \rho = 1\,000\,\mathrm{kg/m^3},$$
$$A = 5{\cdot}07 \times 10^{-4}\,\mathrm{m^2}, \quad m = 0{\cdot}582\,\mathrm{kg/m}, \quad M = 0{\cdot}507\,\mathrm{kg/m}, \quad EI = 5{\cdot}59 \times 10^{-2}\,\mathrm{N\,m^2}, \quad (2a)$$

where ρ_c is the cylinder density, leading to the following dimensionless values:

$$\mathscr{U} = \left(\frac{\rho A}{EI}\right)^{1/2} UL \approx 1{\cdot}57U, \quad \beta = \frac{\rho A}{m + \rho A} \approx 0{\cdot}47,$$
$$\gamma = \frac{(m - \rho A)gL^3}{EI} \simeq 1{\cdot}9, \quad \varepsilon = \frac{L}{D} \approx 20{\cdot}47. \quad (2b)$$

All symbols are defined in Part 2 (Lopes *et al.* 2002).

Furthermore, we assume that $\chi = 1$ and $h = 0$, which corresponds to a cylinder in unconfined flow, and that the friction coefficient $c_d = 0$. For convenience, the tapering-end parameter f and the base drag coefficient c_b are related as per Païdoussis (2002) by $c_b = 1 - f$.

The tapering end is quasiellipsoidal, of length l. The function giving the relation between the diameter and the curvilinear coordinates is $D(s) = D\sqrt{1 - (s - L + l)^2/l^2}$. So, for an ellipsoidal end we have $s_e = \frac{2}{3}l$ and $\bar{s}_e = (\pi/4)l$, and for $l/L = 0{\cdot}01$ we obtain the dimensionless values $\chi_e \approx 6{\cdot}67 \times 10^{-3}$ and $\bar{\chi}_e \approx 7{\cdot}85 \times 10^{-3}$ [see equations (65) and (68) of Lopes *et al.* (2002) for definitions].

As the maximum flow velocity of the water tunnel is around 6 m/s, the corresponding dimensionless one, $\mathscr{U}$, is around 10. Finally, in order to obtain the system period from the dimensionless period, we use the following relationship:

$$t = [(m + M)/EI]^{1/2} L^2 \tau = 1{\cdot}19\tau. \tag{2c}$$

In subsequent sections, all parameters are dimensionless and are set to the values stated above, unless otherwise specified.

2.2. Method of Solution

Depending on the type of analysis and results sought, two different numerical schemes have been used. The first one is based on the Finite Difference Method (FDM) which has been discussed in detail by Semler *et al.* (1996). It is an "initial-value problem solver", which means that the system of equations is integrated numerically for one initial condition at a time, and it is capable of reproducing the state of the system thereafter at any time, τ. The final steady-state represents a *stable attractor*, i.e., a physically possible state.

The second solution scheme involves the use of AUTO (Doedel & Kernéves 1986) which is based on a collocation method. It is adapted to solving continuation and bifurcation problems for differential equations. It determines the stability and the instability of static and periodic solutions, by computing eigenvalues and Floquet multipliers of a known solution.

2.3. Study of Convergence

As already mentioned, the original partial differential equation has been discretized using the Galerkin method. This means that a sufficient number of comparison functions, N, must be used in the discretization. Solutions of equation (1) need to be found for increasing values of N till the solution does not change any more, both qualitatively and quantitatively. It can be shown that this value varies with the different parameters, the major one being the flow velocity. A complete convergence study has been performed by Augu (1999). For the linear problem, it has been proved that for dimensionless flow velocities $\mathscr{U} \leq 10$, $N = 4$ is a good approximation, while for $10 < \mathscr{U} < 15$, $N = 6$ is necessary; so, these are the values that are used in the stability analysis. As will be seen, the situation is more complex for the nonlinear analysis, but generally six modes ($N = 6$) are used for $\mathscr{U} < 11$, and 8–12 modes for $\mathscr{U}$ up to 15, in order to achieve proper convergence.[†]

[†] Depending on the "complexity" of the solutions (e.g., in the vicinity of doubly degenerate bifurcation points), the number of modes required may be high, even at low flow velocities.

3. STABILITY ANALYSIS

Local bifurcations occur when some eigenvalue of the linearized system crosses the imaginary axis. It is therefore of interest to study the behaviour of the linearized system about its equilibrium position as a function of the system parameters. Consequently, the linear system represented by the matrices $[M]$, $[C]$, $[K]$ of dimension N is transformed into a first-order system of dimension $2N$, and the stability analysis is reduced to the evaluation of the eigenvalues of the corresponding matrix: a Hopf bifurcation occurs when a pair of complex conjugate eigenvalues crosses the imaginary-eigenvalue axis, and a pitchfork bifurcation occurs when one eigenvalue becomes equal to zero.

In the system of equations, the following four main parameters are varied and the rest are kept constant: the flow velocity, $\mathscr{U}$, the free-end streamlining parameter, f, the mass ratio, β, and the ratio of the friction coefficients c_N/c_T. In order to reduce the number of figures in the paper, the influence of the different parameters has been summarized on three different plots in which all parameters are fixed, except two: the flow velocity and one of the three others. It is then possible to define areas of stability and instability that can occur, either by divergence or by flutter. This is what is presented next.

3.1. Influence of f

This free-end shape parameter is related to how well streamlined the free end is: $f = 0$ corresponds to a very blunt end, and $f = 1$ to a perfectly well-streamlined tapering end. However, the degree of streamlining also affects c_b; thus, for a blunt end, the base drag is higher. That is why we have taken $c_b = 1 - f$ (Païdoussis 2002; Païdoussis *et al.* 2002). The influence of f is shown in Figure 1. It can be seen that, depending on the value of f, the stability of the system changes dramatically. For example, if $f = 0{\cdot}30$, the cylinder is always stable, which means that it hangs vertically downwards, at its central equilibrium state. For a slightly larger f, say $f = 0{\cdot}35$, first-mode divergence and second-mode flutter are missed out (the lowest two loops of instability in the figure), and the first instability encountered is third-mode flutter; there is also a higher-mode divergence within this flutter boundary.

For higher f, e.g., $f = 0{\cdot}6$, the dynamical behaviour with increasing $\mathscr{U}$ is as follows: (i) the system loses stability by divergence, (ii) it regains stability, (iii) it becomes subject to second-mode flutter, (iv) it is restabilized, (v) it develops third-mode flutter; and (vi) more complex dynamical behaviour then follows.[†] For still higher f, e.g., $f = 0{\cdot}85$, there is no restabilization after the initial loss of stability.

A few distinctive regions need to be mentioned, because they give rise to some interesting behaviour: (i) for $f = 0{\cdot}82$ (region A), the Hopf and the pitchfork bifurcations occur simultaneously, and in such a situation, it is well-known that "nonstandard" behaviour might arise (Païdoussis & Semler 1993*b*); (ii) around regions B, the small loop indicates the emergence of a new periodic solution prior to the disappearance of the existing periodic solutions; hence, in these regions, various possible solutions coexist, which may lead to "complicated" behaviour; and (iii) regions C correspond to the sudden disappearance of Hopf bifurcations.

All these regions are "revisited" in Section 4 since they are "nonlinear" by nature, hence belonging to the "nonlinear" dynamics section.

[†] For this system, some of the higher-mode instabilities do materialize, as seen in Part 1, unlike the internal flow system (Païdoussis 1998); hence this discussion is not entirely academic.

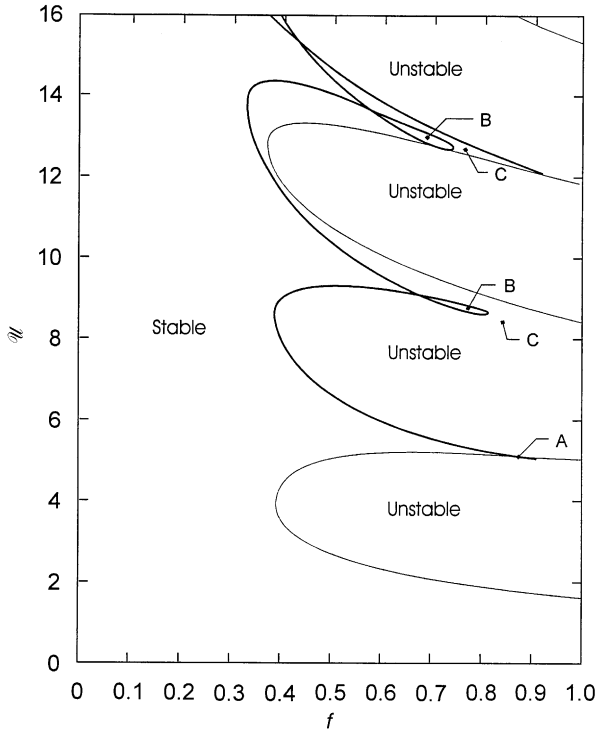

Figure 1. The dynamical behaviour of a cantilevered system ($\beta = 0{\cdot}47$, $\varepsilon c_N = \varepsilon c_T = 0{\cdot}5$, $\gamma = 1{\cdot}9$, $c_b = 0{\cdot}3$, $\chi_e = 0{\cdot}00667$, $\bar{\chi}_e = 0{\cdot}00785$, $c_d = 0$, $\chi = 1$ and $h = 0$), as a function of f; light lines represent the bounds of divergence, while heavier ones those of flutter.

3.2. Influence of β

Figure 2(a) shows the effect of β on stability for a system with $f = 0{\cdot}7$ and otherwise the same parameters, other than β, as in Figure 1. The shaded regions are stable. It is recalled that, similarly to f, the possible range for β is $0 < \beta < 1$—although, realistically, it is from $\sim 10^{-3}$ for a light-gas flow over a heavy cylinder to $\sim 0{\cdot}7$ for a dense fluid flowing over a hollow cylinder; for $\beta > 0{\cdot}7$ approximately, the cylinder would begin to behave as a shell.

Consider the case of $\beta = 0{\cdot}49$ first. The system remains stable up to $\mathscr{U} = 2{\cdot}1$, losing stability by divergence; it is restabilized at $\mathscr{U} = 5{\cdot}2$, and then loses stability by flutter at $\mathscr{U} \sim 5{\cdot}6$; after that, it never regains stability, being subject to different types of flutter and divergence. For larger β, there may be a third range of stability. For $\beta < 0{\cdot}38$, on the other hand, the system never regains stability after divergence, going directly into second- and higher-mode flutter.[†] The horizontal line at $\mathscr{U} = 9{\cdot}6$ represents the onset of the second zone of divergence, and $\mathscr{U} = 12{\cdot}8$ marks its cessation. Note that static instabilities are independent of β.

The perplexing figure-of-eight behaviour is clarified in Figure 2(b), where it is seen how the locus of the flutter mode evolves with varying f, initially as a single instability-restabilization loop for $f = 0{\cdot}5$ and $0{\cdot}6$, to a figure-of-eight closed loop for $f = 0{\cdot}8$ in this case of $\varepsilon c_f = 1$ and $\gamma = 0$ [whereas $\varepsilon c_f = 0{\cdot}5$, $\gamma = 1{\cdot}9$ in Figure 2(a), and the figure-of-eight behaviour arises for $f = 0{\cdot}7$].

[†] See also Section 4.4.

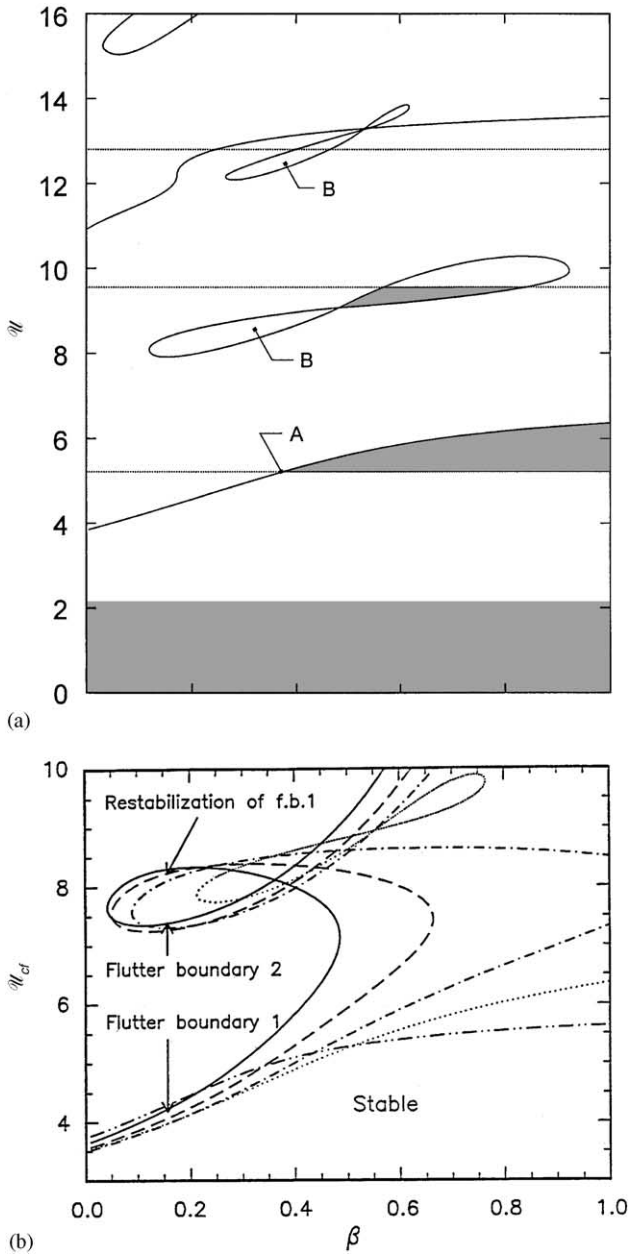

Figure 2. (a) The dynamical behaviour of the same system as in Figure 1, but with f fixed at $f = 0{\cdot}7$ and β variable; the shaded areas are zones of stability. (b) The dynamical behaviour of essentially the same system but with $\varepsilon c_N = \varepsilon c_T = 1$ and $\gamma = 0$, for several values of f, as follows: —, $f = 0{\cdot}5$; – – –, $f = 0{\cdot}6$; —·—·—, $f = 0{\cdot}7$; · · ·, $f = 0{\cdot}8$; —··—··—, $f = 0{\cdot}9$. Note that the figure-of-eight in (b) is a dotted line ($f = 0{\cdot}8$), but the dots are dense, and hence the line may appear to be continuous.

3.3. Influence of c_N/c_T

The effect of f together with εc_N and εc_T for $c_N/c_T = 0{\cdot}5$, 1 and 2, is shown in Figure 3 for divergence and Figure 4 for flutter. In Figure 3, in addition to the first divergence zone,

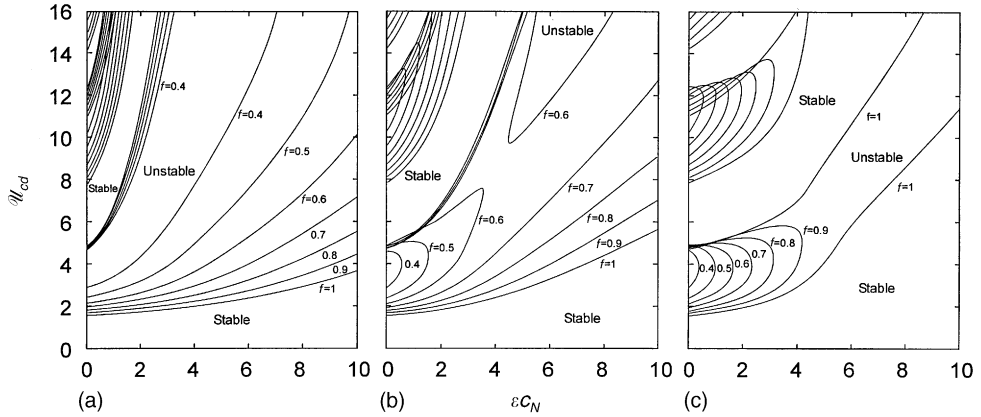

Figure 3. The effect of varying εc_N on $\mathscr{U}_{cd}$ for various values of f, and $\beta = 0{\cdot}47$, $\chi = 1$, $c_b = 1 - f$, $\chi_e = 0{\cdot}00667$, $\bar{\chi}_e = 0.00785$, $\gamma = 0$, for (a) $c_N/c_T = \frac{1}{2}$; (b) $c_N/c_T = 1$; (c) $c_N/c_T = 2$.

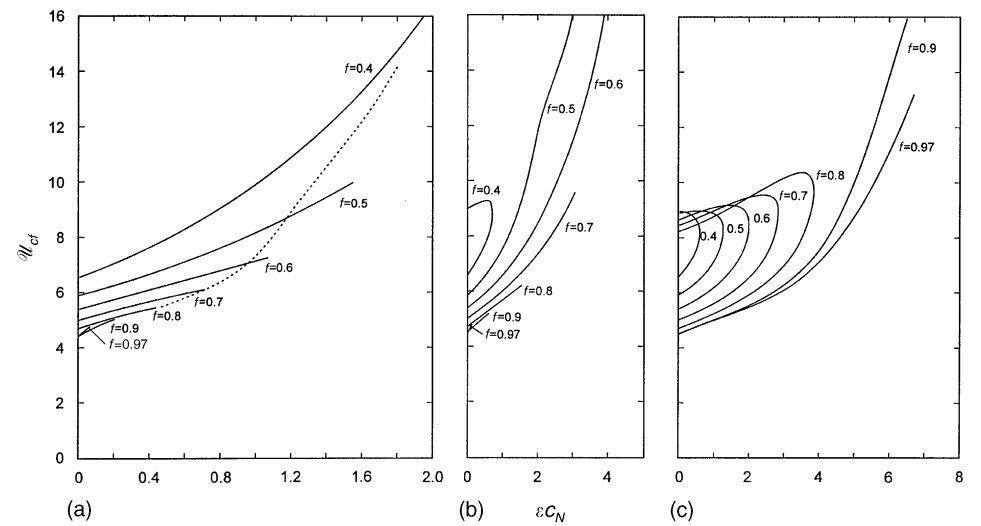

Figure 4. The effect of varying εc_N on $\mathscr{U}_{cf}$ for second-mode flutter, for various values of f, and $\beta = 0{\cdot}47$, $\chi = 1$, $c_b = 1 - f$, $\chi_e = 0{\cdot}00667$, $\bar{\chi}_e = 0{\cdot}00785$, $\gamma = 0$, for (a) $c_N/c_T = \frac{1}{2}$; (b) $c_N/c_T = 1$; (c) $c_N/c_T = 2$: —, flutter via a Hopf bifurcation; - - -, "Païdoussis-type" flutter (Païdoussis 1998), shown for $f = 0{\cdot}8$, $c_N/c_T = \frac{1}{2}$ only.

one can see a second and the beginnings of a third one; most clearly in Figure 3(a). On the other hand, only the first (second-mode) flutter zone is shown in Figure 4.

In Figure 4(a, b) it would appear that flutter abruptly disappears for high enough εc_N when f is high. This is not true. The results in Figure 4 have been obtained using AUTO (Doedel & Kernéves 1986), which can only detect flutter via a Hopf bifurcation. For high εc_N and f, however, the flutter is of the coupled-mode variety, i.e., the eigenvalues λ do not cross the imaginary axis with a nonzero complex part, but with two positive real eigenvalues coalescing and giving rise to two complex-conjugate eigenvalues with positive real part [Païdoussis (2002); cf. Païdoussis (1998, Figure 3.4(d))]. In one case, for $f = 0{\cdot}8$ in Figure 4(a), the values of $\mathscr{U}_{cf}$ for coupled-mode flutter have been added (dashed line), and

are seen to follow smoothly those for single-mode flutter. This is true for all cases, but the calculations are tedious and the curves for other f have not been similarly extended.

It is clear from Figures 3 and 4 that, provided εc_N is sufficiently small, say $\varepsilon c_N < 0{\cdot}2$, its effect on both $\mathscr{U}_{cd}$ and $\mathscr{U}_{cf}$ is quite small, as to a lesser extent is the effect of varying c_N/c_T. This, however, is not true for very small f and for larger values of εc_N, when both εc_N and c_N/c_T influence the dynamics quite significantly.

In general terms, increasing εc_N stabilizes the system in both divergence and flutter. For high enough εc_N and low enough f, divergence may be suppressed altogether, e.g., for $\varepsilon c_N = 2$ and $f = 0{\cdot}5$ in Figure 3(b, c). This is also true for flutter. Also, again generally, increasing c_N/c_T stabilizes the system for divergence [e.g., cf. $\mathscr{U}_{cd}$ for $\varepsilon c_N = 2$ and $f = 0{\cdot}7$ in Figure 3(a–c)]; this stabilization becomes more significant at higher values of εc_N, e.g., for $\varepsilon c_N = 6$. On the other hand, increasing c_N/c_T is destabilizing for flutter [e.g., cf. $\mathscr{U}_{cf}$ for $\varepsilon c_N = 1$ and $f = 0{\cdot}6$ in Figure 4(a–c)]. However, there are exceptions to these general observations, e.g., because the instability curves become closed in some cases, as in Figures 3(b, c) and 4(b, c).

4. NONLINEAR ANALYSIS

Whereas linear analysis of the system can only predict the instabilities emanating from the initial (trivial) configuration since it is based on small motions, nonlinear analysis may provide a fuller, deeper understanding of the dynamics of the system, as discussed in detail in Païdoussis (1998). For example, it is possible to determine if the bifurcations are sub- or supercritical, to see if "secondary" bifurcations materialize, and to find the amplitudes of the oscillations or of the static solutions. This information is usually graphically summarized in a bifurcation diagram, where the amplitude of the system is plotted as a function of one parameter, the flow velocity in this case. One such bifurcation diagram is presented in Figure 5 where many interesting dynamical features may be observed.[†] The convention in this figure is as follows: a solution on the x-axis represents the original configuration, i.e., the inert cylinder hanging downwards. A nonzero solution can represent either a nontrivial static equilibrium position (representing a buckled stationary cylinder) or the amplitude of oscillation for flutter. Moreover, these solutions can be either stable (drawn as heavy, continuous lines), meaning that they can be observed physically, or unstable, in which case they are not physically possible (drawn as thin, continuous or dotted lines).

As is well known, bifurcations are determined mathematically by the eigenvalues in the case of a fixed point (denoted by λ, with $\lambda = 0$ or $\lambda = \pm \mathrm{i}\omega$), and by the Floquet multipliers in the case of a periodic solution (denoted by Λ, with $\Lambda = +1, -1$ or complex conjugate with $|\Lambda| = 1$). A complete description may be found in Païdoussis (1998). Figure 5 has been obtained with AUTO, with $N = 6$ for $\mathscr{U} < 9$ and with $N = 8$ for higher flow velocities, and with the first generalized coordinate q_1 being representative of the behaviour of the system. In order to simplify the discussion, the results have been subdivided into different sections: (i) $\mathscr{U} < 9$, (ii) $\mathscr{U} > 9$ and (iii) $\mathscr{U} \sim 8{\cdot}6$.

[†] Figure 5 has been obtained with the form of the equations obtained in Lopes *et al.* (1999); see Section 4.2 and Appendix A of Part 2. As discussed in Part 2, because $h = 0$ and $\gamma = 1{\cdot}9$ in this case, the difference between these results and those with the refined, corrected version of the equation of motion, equation (54) of Part 2, is expected to be minimal; this figure was nevertheless not recalculated using equation (54), because of the heavy investment of computational time this would entail.

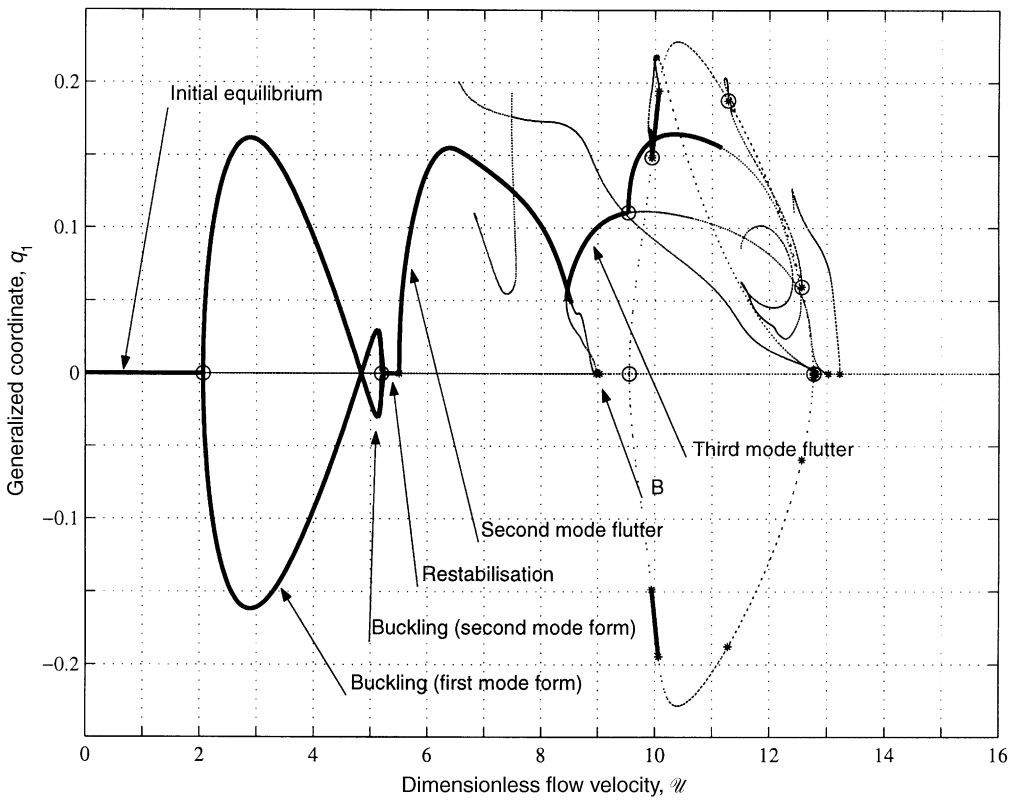

Figure 5. Typical bifurcation diagram for $\beta = 0{\cdot}47$, $f = 0{\cdot}7$, $\gamma = 1{\cdot}9$, $\varepsilon c_N = \varepsilon c_T = 0{\cdot}5$, $c_b = 0{\cdot}3$, $\chi_e = 0{\cdot}00667$, $\tilde{\chi}_e = 0{\cdot}00785$, $c_d = 0$, $\chi = 1$ and $h = 0$, with $N = 6$ (for $\mathscr{U} < 9$) and $N = 8$ modes in the Galerkin approximation, showing the first generalized coordinate, q_1, as a function of $\mathscr{U}$: —, stable solutions; —, · · ·, unstable solutions.

4.1. Dynamics for $\mathscr{U} < 9$

From Figure 5, the dynamics of the system for $\mathscr{U} < 9$ may be summarized as follows.

(i) As expected, the zero solution corresponding to the original equilibrium state is stable; this is so, up to $\mathscr{U} = 2{\cdot}1$. At this flow velocity, a supercritical pitchfork bifurcation corresponding to one eigenvalue equal to zero ($\lambda = 0$) occurs, leading to divergence in the first mode; q_1 subsequently increases with $\mathscr{U}$.

(ii) For $\mathscr{U} > 3$ approximately, q_1 begins to decrease, reaches zero, and then increases again over a small range of $\mathscr{U}$. This is because, with increasing $\mathscr{U}$, the first-mode divergence slowly changes into a second-mode-shape divergence. Subsequently, for $\mathscr{U} > 5{\cdot}25$, the system is restabilized over a short range of flow velocities through a subcritical pitchfork bifurcation ($\lambda = 0$ at $\mathscr{U} = 5{\cdot}25$).

(iii) Almost immediately after, at $\mathscr{U} = 5{\cdot}5$, the trivial "zero" solution loses stability again through a supercritical Hopf bifurcation ($\lambda = \pm \mathrm{i}\omega$) which leads to flutter in the second mode, corresponding to periodic oscillations around the origin.

(iv) This periodic solution becomes unstable through a torus bifurcation (two complex-conjugate Floquet multipliers cross the unit circle, i.e., $\Lambda = a \pm \mathrm{i}b$ with $|\Lambda| = 1$) at $\mathscr{U} = 8{\cdot}52$ prior reaching the x-axis at $\mathscr{U} = 8{\cdot}97$. The "$|\Lambda| = 1$" bifurcation usually corresponds to the appearance of a second frequency in the periodic response, i.e., to quasiperiodic

solutions which cannot be "followed" by AUTO. Moreover, this unstable solution can also be seen as emerging from a subcritical Hopf bifurcation of the origin at $\mathscr{U} = 8{\cdot}97$, i.e., with $\lambda = \pm i\omega$.

(v) Just before the aforementioned bifurcation, an unstable third-mode flutter solution arises from a subcritical Hopf bifurcation of the trivial solution at $\mathscr{U} = 8{\cdot}94$. This unstable solution becomes stable at $\mathscr{U} = 8{\cdot}44$ through a saddle-node bifurcation ($\Lambda = +1$), which corresponds to a turning or limit point (Moon 1992). So, again, stable periodic solutions may be seen.

A few additional comments on the dynamical behaviour of the system may be useful.

(i) Physically, and in general, the following sequence is predicted: (α) the stable initial equilibrium ($q_1 = 0$) is succeeded by (β) static divergence in the first mode ($q_1 \neq 0$), then it is transformed to (γ) divergence in the second mode; (δ) this is followed by a return to stability at the initial equilibrium ($q_1 = 0$), (ε) oscillatory (periodic) motion in the second mode and (ζ) oscillatory motion in the third mode. This is illustrated in Figure 6, where the shape of the cylinder is shown as a function of time for some representative cases. For $\mathscr{U} = 3$, the cylinder does not oscillate and its shape is similar to that of the first eigenmode of a cantilevered beam [Figure 6(a)—corresponds to state (β)]. For $\mathscr{U} = 5$, the amplitude is much smaller and the shape is similar to the second eigenmode of a cantilevered beam, there being an inflexion point in the curve [Figure 6(b)—state (γ)]. For $\mathscr{U} = 6$, the cylinder oscillates and the shape again corresponds to a second eigenmode [Figure 6(c)—state (ε)]. Finally, for $\mathscr{U} = 9$, the cylinder oscillates with a high contribution of the third mode [Figure 6(d)—state (ζ)].

(ii) The transition between the second and the third mode needs further discussion, since more than one stable solution may exist over a small range of $\mathscr{U}$. This is discussed in Section 4.3.

(iii) From Figure 5, it is obvious that linear and nonlinear analyses yield different results; this is the case because some bifurcations are subcritical, which means that "nonlinear solutions" exist for flow velocities below the bifurcation points predicted by linear theory.

(iv) Nevertheless, because the system is restabilized prior to the dynamic instability, predictions by linear theory are, in fact, quite adequate for flow velocities below $\mathscr{U} = 8$, which explains why agreement between linear theory and experiments is indeed "good" (Païdoussis *et al*. 2002).

(v) The sequence found, i.e., {stability} → {divergence} → {stability} → {oscillation in the second mode} → {oscillation in the third mode}, is essentially the same as described in the experiments (Païdoussis *et al*. 2002), which is very satisfactory; further discussion is presented in Section 5.

(vi) Of course, the results shown here are valid quantitatively only for the parameters chosen. Nevertheless, these parameters are representative of what has been obtained over a much larger range. A complete investigation may be found in Lopes *et al*. (1999) and Augu (1999).

4.2. Dynamics for $\mathscr{U} > 9$

For $\mathscr{U} > 9$, the bifurcation diagram, and hence the dynamical behaviour, becomes more complicated. Indeed, from Figure 5, it is possible to see many different solution branches, most of them unstable. The third-mode flutter discussed previously becomes unstable at $\mathscr{U} = 9{\cdot}57$ through a pitchfork bifurcation ($\Lambda = +1$) which breaks the symmetry of the response with respect to the x-axis. This gives rise to two new solutions, one being unstable and one stable. Physically, corresponding to the stable solution after $\mathscr{U} = 9{\cdot}57$,

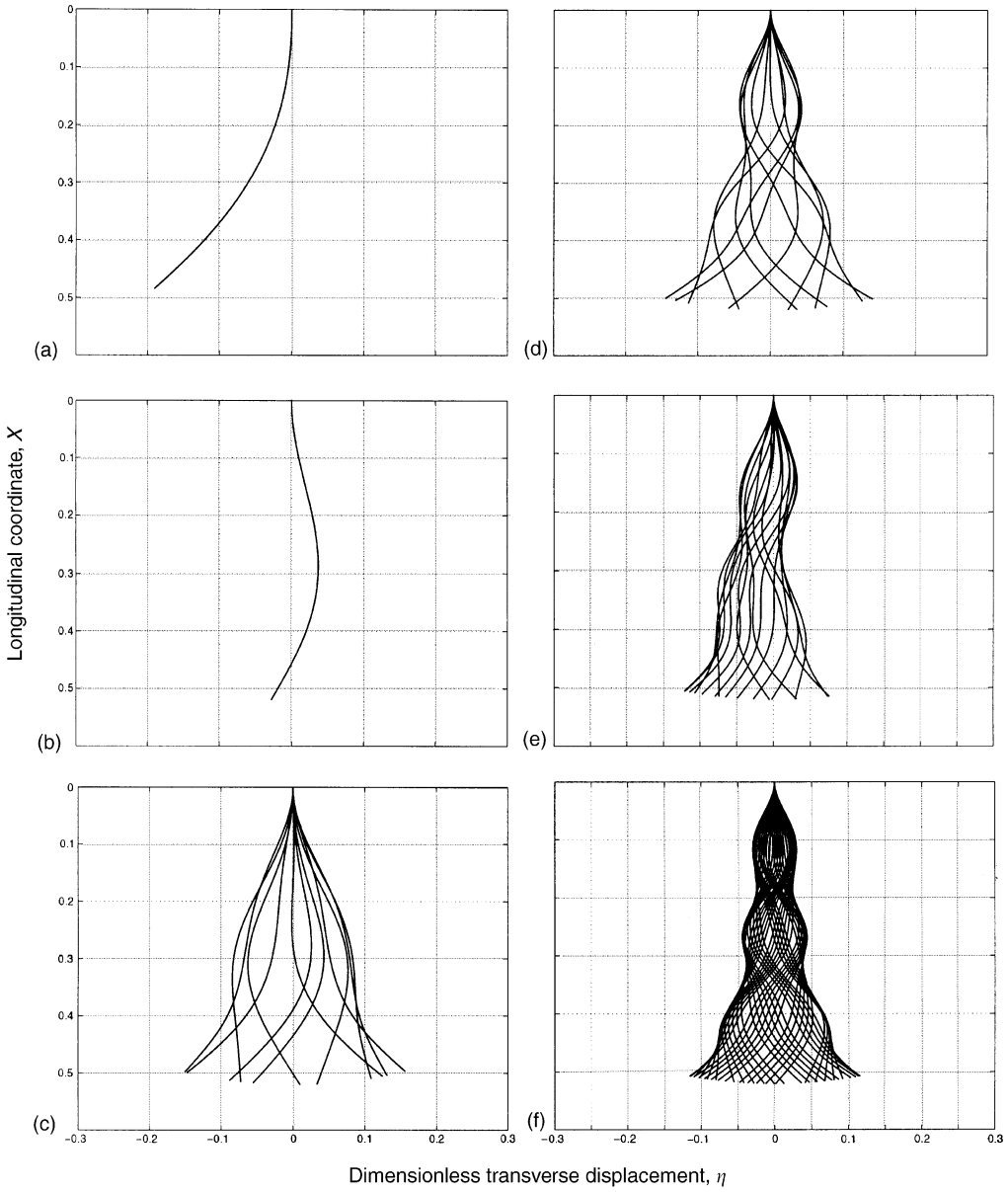

Figure 6. Shape of the cylinder for various values of the dimensionless flow velocity, $\mathscr{U}$, and for the same parameters as in Figure 5: (a) first-mode divergence (buckling) at $\mathscr{U} = 3$, (b) second-mode (shape) buckling at $\mathscr{U} = 5$, (c) second-mode flutter at $\mathscr{U} = 6$, (d) third-mode flutter at $\mathscr{U} = 9$, (e) third-mode flutter around a buckled position (combination of buckling and flutter leading to an asymmetric response) at $\mathscr{U} = 11{\cdot}8$, (f) fourth-mode flutter at $\mathscr{U} = 13{\cdot}7$, but with $f = 0{\cdot}6$ instead of $f = 0{\cdot}7$. The last two figures have been computed with $N = 12$.

the cylinder oscillates around a new equilibrium, which means that divergence and flutter coexist in the response. This is similar to what has been observed by Païdoussis & Semler (1993*b*) for the dynamics of a cantilevered pipe with an intermediate spring support, conveying fluid. The new stable solution also becomes unstable at $\mathscr{U} = 11{\cdot}16$, so that, apparently, no periodic solution exists thereafter. However, for $\mathscr{U} > 9$, the bifurcation

diagram of Figure 5 has been obtained for $N = 8$ (eight-mode approximation). From a computational point of view, this has been the maximum that could be used in conjunction with AUTO. Hence, because "fourth-mode" solutions have been observed by Païdoussis *et al*. (2002), and because a thorough study of Figure 1 intuitively suggests that it might be possible to obtain them numerically, it has been decided to use FDM to integrate directly the equations of motion with $N = 12$ modes. Some sample phase-plane plots are given in Figure 7 and some additional cylinder shapes in Figure 6(e, f).

At $\mathscr{U} = 11{\cdot}8$, the response in Figure 7(b) is periodic but nonsymmetric, in contrast to the case of $\mathscr{U} = 6$ shown in Figure 7(a). Later, a period-doubling bifurcation occurs ($\Lambda = -1$) and a double loop can be observed [Figure 7(c)]. This new stable solution again loses stability through another period-doubling bifurcation, leading to "period-four" oscillations, as illustrated in Figure 7(d) for $\mathscr{U} = 12{\cdot}3$. However, rather than seeing the well-known cascade of period-doubling (Païdoussis & Semler 1993*a*), here a "period-bubbling" occurs instead. This leads back to "period-two" [Figure 7(e)] and to "period-one" oscillations [Figure 7(f)], still in the third mode. Hence, through this sequence of bifurcations, no quasiperiodic/chaotic motion could be found.

At higher flows, fourth-mode oscillations could be found [e.g., for $f = 0{\cdot}6$ and $\mathscr{U} = 13{\cdot}7$, as in Figure 6(f)]; the transition from third to fourth mode is supposed to follow the same pattern as described for the second-to-third mode transition in the section that follows.

4.3. Dynamics in the Transition Region $\mathscr{U} \sim 8{\cdot}6$

In Sections 4.1 and 4.2, most of the dynamics has been captured, explained and illustrated. Nevertheless, there is a small range of $\mathscr{U}$ of interest for which "atypical" behaviour can be observed, because of the presence of different stable attractors. For clarity, a zoomed version of the bifurcation diagram of Figure 5 is given in Figure 8(a): not only are the different periodic solutions clearer (both stable and unstable), but it is also possible to see that there is a small region for which both second- and third-mode flutter solutions are stable. Figure 8(a) has been obtained by AUTO, which is not able to take the initial conditions into account (it simply follows a previously known solution). Hence, FDM has been used to see if indeed these two solutions could be found. This, in fact, is so. The two possible attractors for $\mathscr{U} = 8{\cdot}50$ are displayed in Figure 8(b), obtained with two different initial conditions, which confirms the accuracy of both (numerical) solutions.

As already mentioned, at $\mathscr{U} = 8{\cdot}52$, the second-mode flutter becomes unstable through a torus bifurcation ($\Lambda = a \pm ib$ with $|\Lambda| = 1$). Thus, in theory, quasiperiodic solutions are possible. This is illustrated in Figure 8(c), where again two different attractors are displayed (for two sets of initial conditions), for $\mathscr{U} = 8{\cdot}53$, i.e., just after the bifurcation. The aperiodic solution is sensitive to the initial conditions and is mainly composed of two unstable solutions. It is definitely proved, through power spectral density calculations, but mainly through Poincaré sections such as shown in Figure 8(d), that the response converges either to the third-mode limit cycle or to the "nonperiodic" attractor.

This transition has been observed near regions B of Figure 1, but similar behaviour has been observed for different parameters in the C regions (a B region corresponds to the appearance of the third-mode solution before the disappearance of the second-mode solution, while in regions C the two Hopf bifurcations of the original equilibrium, i.e., from a linear point of view, disappear completely). For example, the C region exists for $\beta = 0{\cdot}6$ and $f = 0{\cdot}8$, for which a bifurcation diagram is shown in Figure 9: even though no solution emerges from the original equilibrium, the dynamics is still very similar. From the results obtained using either AUTO (stable and unstable solutions shown in Figure 9) and

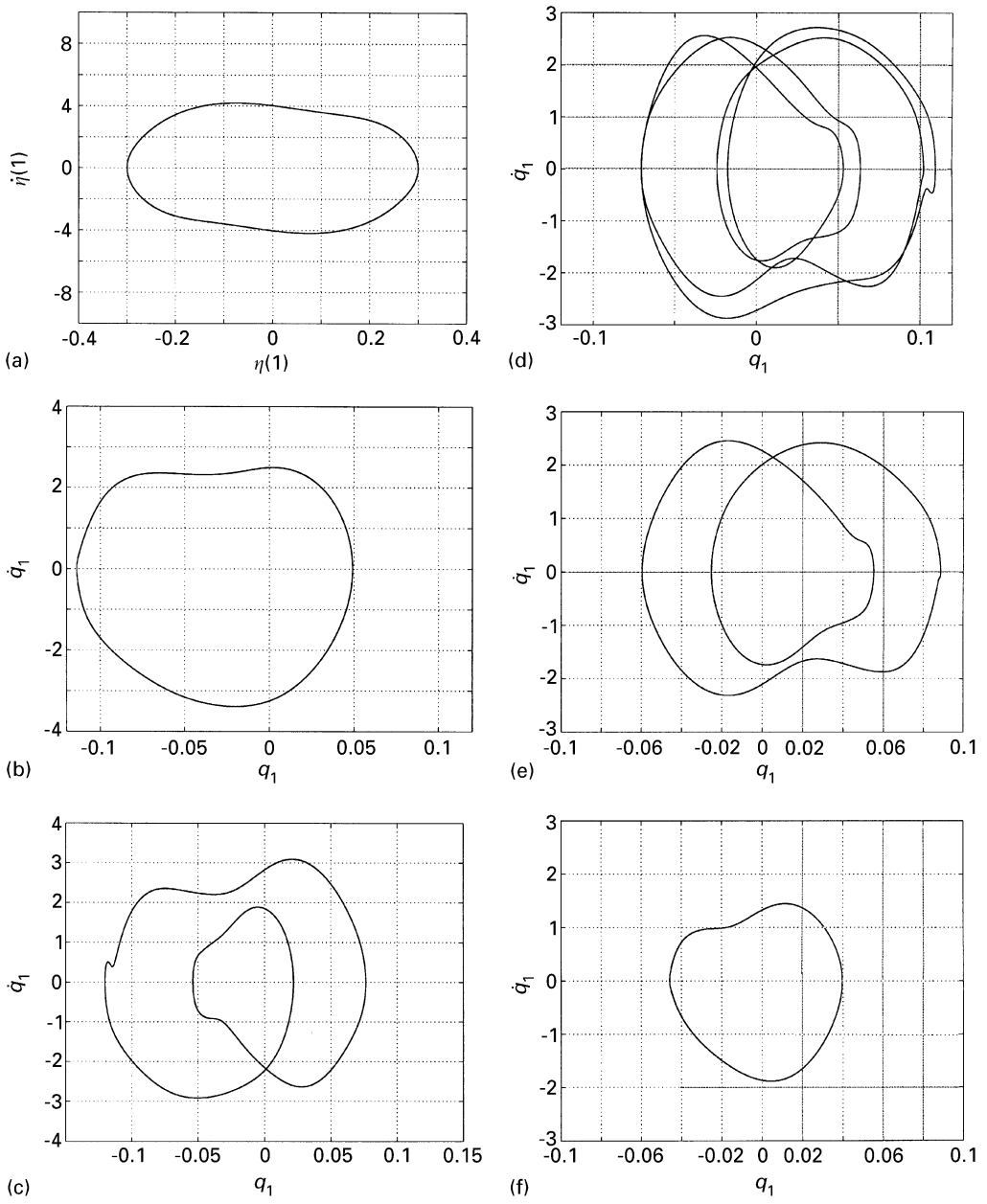

Figure 7. Phase-plane plots for various values of $\mathscr{U}$ demonstrating the transition between third- and fourth-mode flutter, for the same parameters as in Figure 5: (a) "symmetric" response for $\mathscr{U} = 6$ [corresponds to Figure 6(c)]; (b) "asymmetric" response for $\mathscr{U} = 11{\cdot}8$ [see Figure 6(e)]; (c) period-two oscillations for $\mathscr{U} = 12{\cdot}2$; (d) period-four oscillations for $\mathscr{U} = 12{\cdot}3$; (e) period-two oscillations with a higher frequency for $\mathscr{U} = 12{\cdot}4$; (f) third-mode flutter ("period one") for $\mathscr{U} = 12{\cdot}8$. (b–f) show clearly the "period-bubbling" phenomenon.

FDM (not shown), the following sequence has been observed: periodic solution at $\mathscr{U} = 8{\cdot}50$, quasiperiodic solution at $\mathscr{U} = 8{\cdot}67$ (corresponding to the discontinuity in the curve in Figure 9), followed by periodic motions at $\mathscr{U} = 8{\cdot}70$, and then third-mode flutter

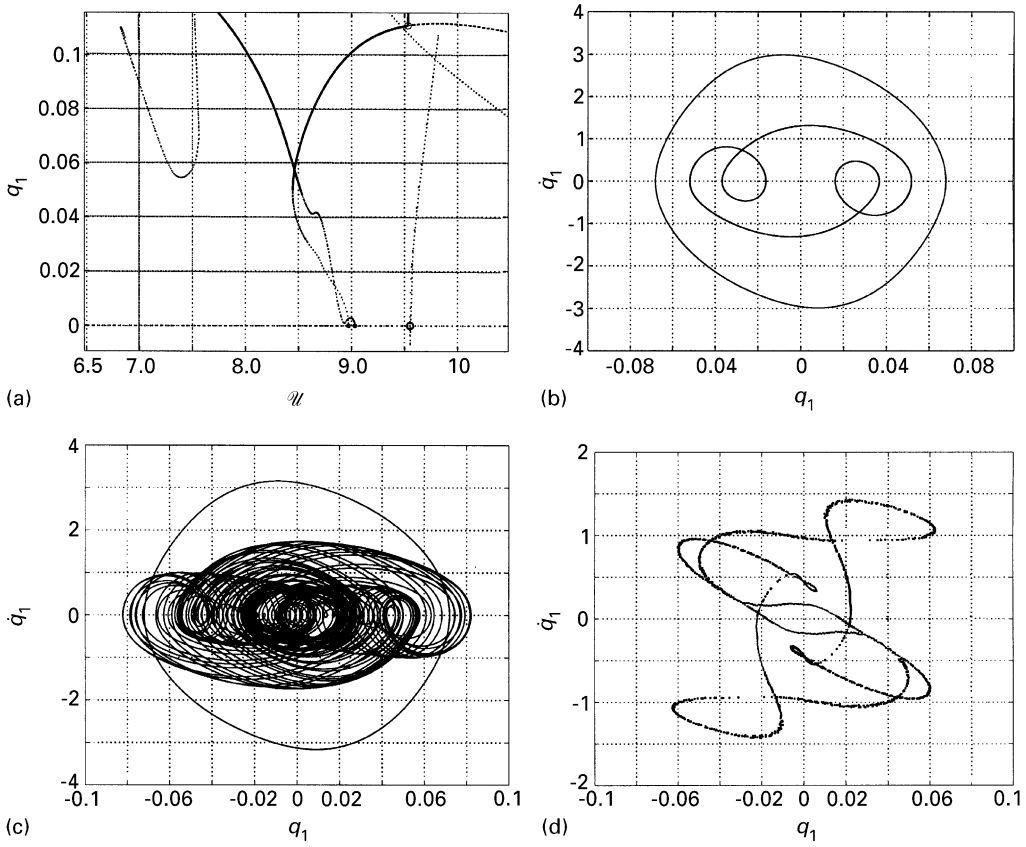

Figure 8. Dynamics in the transition region, $\mathscr{U} \sim 8{\cdot}6$: (a) zoomed version of Figure 5 in the region of interest obtained with AUTO; (b) phase-plane plot for two initial conditions showing the coexistence of the two periodic solutions, at $\mathscr{U} = 8{\cdot}50$; (c) phase-plane plot showing the periodic and the nonperiodic attractors, at $\mathscr{U} = 8{\cdot}53$; and (d) Poincaré section representing the trace of the quasiperiodic attractor.

at $\mathscr{U} \simeq 9{\cdot}0$. Moreover, the quasiperiodic solution is composed of the two flutter modes, even though no limit cycle exists concurrently. Consequently, regions B and C are qualitatively similar since the different transitions are the same.

4.4. Linear Map Revisited

Throughout Sections 4.1–4.3, the nonlinear dynamical behaviour has been described and is now fully understood. In particular, the transitions between the various possible solutions have been explained, and the amplitudes and frequencies of the oscillating cylinder obtained over a wide range parameters. With this understanding, it can be seen that most of the dynamical behaviour can now "easily" be extracted from Figure 1: the regions where the cylinder is stable, where it "buckles", where it flutters in the second or the third mode, and where there exist regions of quasiperiodicity. Consequently, the same logic may be used to predict the behaviour of the system for $\mathscr{U} > 13$ (approximately, and for the values of f of interest) by presuming the existence of some fourth-mode solutions following the third-mode oscillations. Depending on the value of f, it is possible to assume

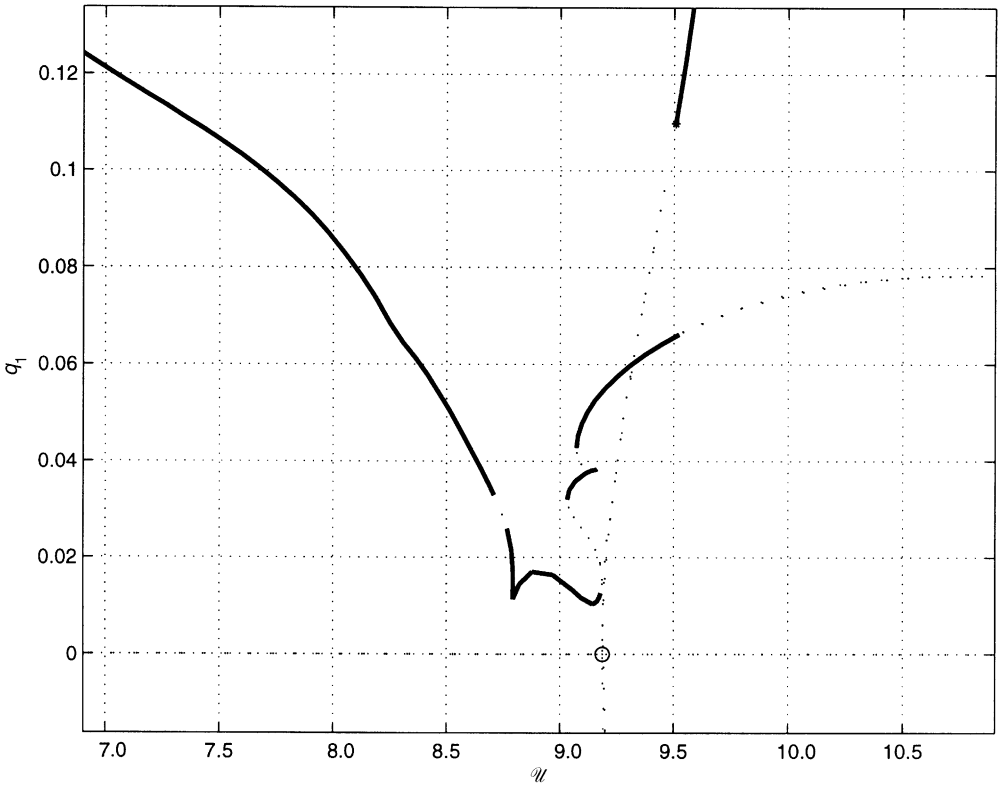

Figure 9. Bifurcation diagram in region C of Figure 1 for which the two Hopf bifurcations do not exist, in the neighbourhood of the "transition zone", showing the first generalized coordinate, q_1, as a function of $\mathscr{U}$: —, stable solutions, · · ·, unstable solutions; $\beta = 0{\cdot}60$, $f = 0{\cdot}8$, $\gamma = 0$, $\varepsilon c_N = \varepsilon c_T = 0{\cdot}5$, $c_b = 1 - f = 0{\cdot}2$, $\chi_e = 0{\cdot}00667$, $\bar{\chi}_e = 0{\cdot}00785$, $c_d = 0$, $\chi = 1$ and $h = 0$, $N = 6$.

that two types of transition leading to a fourth-mode periodic solution are possible: from a stable equilibrium (for $f = 0{\cdot}5$), or from quasiperiodic solutions (for $f = 0{\cdot}7$ through region B where third- and fourth-mode solutions coexist, or for $f = 0{\cdot}75$ through region C where the two Hopf bifurcations do not exist). To verify numerically that these assumptions are valid, a high enough number of modes need to be used in the computation: 13 modes are necessary to find the "appropriate" solution in regions B and C for $12 < \mathscr{U} < 14$. Nevertheless, using 12 modes only, for $\mathscr{U} = 13{\cdot}7$, $f = 0{\cdot}6$ and $\beta = 0{\cdot}47$, it was possible to find a "fourth-mode" solution, as predicted. Needless to say that getting one such solution is very (computer) time consuming.

This leads to the conclusion that the bifurcation diagram in Figure 5 is not correct for $\mathscr{U} > 11$. The correct behaviour is the following: third-mode flutter, followed by period-doubling and then period-bubbling, quasiperiodic behaviour, and finally fourth-mode flutter. The same conclusion applies to Figure 6 in Païdoussis *et al.* (1999).

One final area to describe is the dynamics in the vicinity of point A where the second-mode flutter arises before restabilization of the first-mode buckling. This occurs for example for $\beta < 0{\cdot}39$ in Figure 2(a). Initially, some "burst" phenomena had been described with no explanation by Lopes *et al.* (1999), i.e., regions where no stable periodic solutions were found to exist. Further investigation has shown that this was due to an insufficient number of modes in the calculations: with $N = 12$ and $\beta = 0{\cdot}2$, it is possible to find

periodic oscillations for $\mathscr{U} > 5$, which means that region A is not much different from a dynamics point of view (as originally thought).

5. COMPARISON WITH THE EXPERIMENTS

To give a better appreciation of the results obtained, qualitative and quantitative comparisons between theory and experiment are undertaken. This is presented next.

5.1. Qualitative Comparison

Some typical cylinder shapes, both theoretical and experimental, are presented side by side in Figure 10, for different values of $\mathscr{U}$ and for the same parameters as in Figure 5. The theoretical shapes have been obtained simply through Galerkin's method and using both the computed generalized coordinates, q_j, and the shape functions converted back to a dimensional length. Hence, the length X shown in Figure 10 is dimensional, in order to display cylinder shapes comparable with the experiment. The flow velocity in the theory and in the experiment may be slightly different,[†] which contributes to some of the discrepancies in amplitude.

Figure 10(a, b) represents the case of a first-mode-shape buckling. The theoretical point has been chosen (at $\mathscr{U} = 2{\cdot}8$) such that the amplitude is the largest. This is not necessarily the case in the experiment, but in general, the theoretical amplitude of the first-mode buckling is always larger than the experimental one. This may partly be due to the third-order approximation made when deriving the equation of motion—see Section 2 of Lopes *et al*. (2002). Figure 10(c, d) represents the second-mode shape buckling ($\mathscr{U} = 5{\cdot}2$), and in this case, for smaller amplitudes, good agreement between theory and experiment is observed. This is also the case in Figure 10(e, f) where flutter in the second mode is clearly demonstrated ($\mathscr{U} = 6{\cdot}1$). Finally, flutter in the third-mode is shown in Figure 10(g, h), again very similar between theory (at $\mathscr{U} = 9{\cdot}1$) and experiment.

The equations of motion developed by Lopes *et al*. (2002) being two dimensional, it is of course not possible to capture the three-dimensional motions that have been found by Païdoussis *et al*. (2002). Nevertheless, it is quite possible that quasiperiodic solutions found in theory may develop and may be attracted to a three-dimensional solution with a proper theoretical model that could exhibit that.

5.2. Quantitative Comparison

Comparisons of thresholds of divergence and second-mode flutter obtainable by linear theory (which are identical to those determined from bifurcation diagrams) have been made in Part 1, showing fair agreement with the experiment. Some of these comparisons are summarized in Table 1 here, where some nonlinear features of the behaviour are also compared.

In terms of global behavioural (qualitative) characteristics, Figure 10 clearly shows a parallel between theory and experiment, but a deeper quantitative comparison needs to be undertaken. From relations (2b) and all the results already given, it is obvious that a lot of

[†] Some of the parameters are also different: in the theoretical results, $\gamma = 0$, while in the experiments $\gamma = 1{\cdot}9$. Here it is noted that, since $\gamma = 0$, the theory in Part 2 and that in Lopes *et al*. (1999)—see Appendix A of Part 2—are identical.

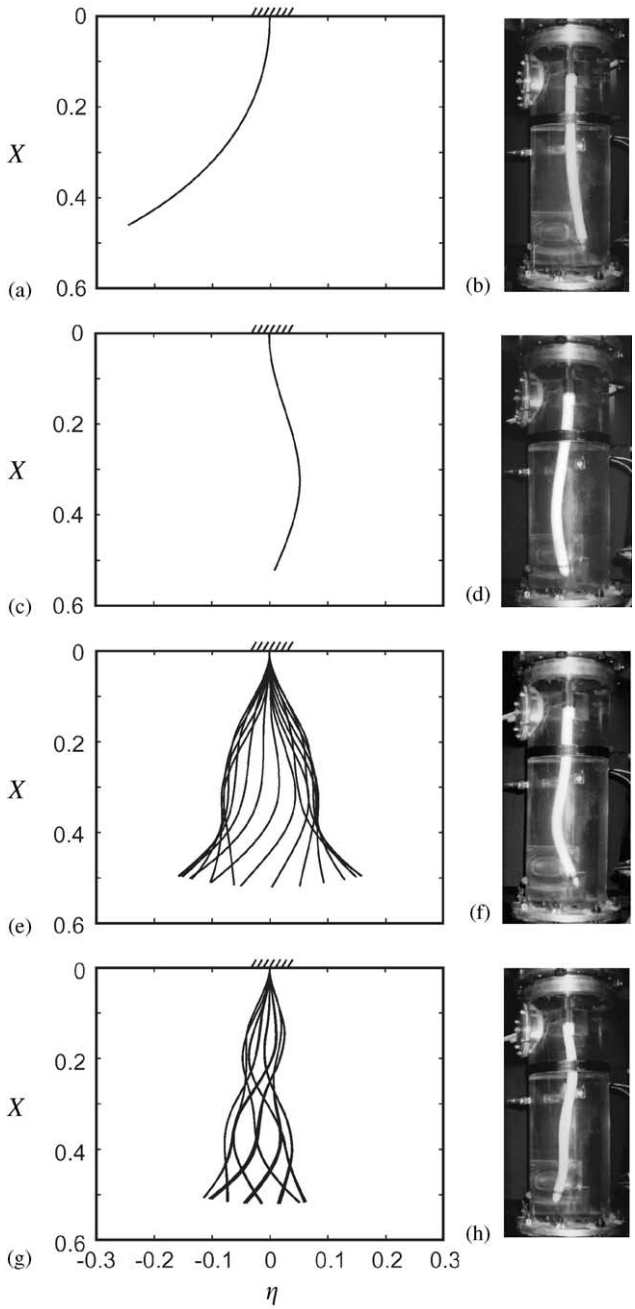

Figure 10. Shape of the cylinder: qualitative comparison between theory (a, c, e, g) and experiment (b, d, f, h) showing successively: buckling of first-mode shape, buckling of second-mode shape, second-mode flutter and third-mode flutter.

parameters may have an influence on the dynamics. Taking different criteria into account, an attempt has been made to reduce the possible range of all parameters by developing a "behavioural" map that would be in accordance with the physical tests. Again, the major parameters chosen are the flow velocity $\mathscr{U}$, the mass ration β, and free-end shape

TABLE 1

Flow velocity for the different bifurcation points: comparison between theory and experiment

Phenomenon	Theory		Experiment	
	$f = 0{\cdot}7$ $\varepsilon c_f = 0{\cdot}5$	$f = 0{\cdot}6$ $\varepsilon c_f = 0{\cdot}25$	Well-streaml. tail	Medium streaml. tail
Divergence threshold, $\mathscr{U}_{cd}$	2·10	2·50	1·8–2·3	2·0–2·7
Divergence, second-mode shape	4·5	?*	4·1–4·4	3·9–4·4
Restabilization	4·79	5·02	—	—
Second-mode flutter threshold, $\mathscr{U}_{cf}$	4·82	6·03	5·1–5·4	5·1–5·7
Quasiperiodic, $\mathscr{U}$	8·50	—	6·9–7·1	7·2–7·4†
Third-mode flutter threshold, $\mathscr{U}$	8·60	8·91	7·0	7·0–7·5†

*Signifies uncertainty as to its existence.
†Or sometimes none.

parameter f. The different criteria are: the "qualitative route" (stability–divergence–flutter–quasiperiodic solution), the bifurcation values for $\mathscr{U}$, the amplitude of motion (both static and dynamic), and the period of oscillation. A detailed analysis may be found in Augu (1999) where it is shown that, to have "good" agreement, the following two conditions need to be satisfied: $0{\cdot}7 < f < 0{\cdot}8$, and $0{\cdot}46 < \beta < 0{\cdot}6$. The mass parameter β can be measured precisely, and for the cylinders used in Païdoussis *et al.* (2002), it is equal to $\beta = 0{\cdot}47$; so, this parameter at least is in the determined range. The parameter f, however, is more difficult to estimate; so, two values are specified in Table 1 for comparison purposes, one even outside the determined range.

For the purposes of Table 1, the free-end shapes #115, #15 and #2 (see Part 1) are considered to be "well streamlined", while #91, #35 and #92 to be "medium well streamlined".

It is seen that the thresholds of divergence and second-mode flutter are in reasonable agreement, although the theoretically predicted restabilization has not been observed;† in practice, in these experiments, the system never really becomes totally straight before the onset of second-mode flutter, although the deformation is of second-mode shape.

It is also seen that third-mode flutter in the experiments occurs at considerably lower $\mathscr{U}$ than predicted, and so does the quasiperiodic behaviour. In the experiments, quasiperiodicity manifests itself as a "hesitation" between second- and third-mode flutter—in appearance similar to chaotic behaviour; in the power spectral density (PSD), there are two or more frequency peaks of similar amplitude. In some cases, quasiperiodic behaviour is not clear or does not occur and this is marked as "sometimes none" in the table.

Here it should be remarked that the theoretical calculations with $N = 6$ are at the limit of being reliable for high values of $\mathscr{U}$ (e.g., $\mathscr{U} > 7$). It has been found, by conducting calculations with fewer degrees of freedom, that increasing N would result in lower values for the bifurcation values of $\mathscr{U}$ for the quasiperiodic behaviour and for the third-mode flutter ($\mathscr{U} > 7$).

†In this respect, it should be said that for slightly different parameters than those chosen, one can obtain theoretical results in which there is no restabilization. E.g., in Figure 2, this can be done by reducing β, which would be nonphysical, since the value of β is certain; however, the same can arise by varying other system parameters, values for which are less well known.

TABLE 2

Comparison between theory and experiment of the maximum nondimensional tip amplitudes and the nondimensional frequency (denoted as Hz^*) of limit-cycle oscillation

Quantity	Theory	Experiment
Max. amplitude at divergence, $\eta(1)_{max}$	0·25	0·10–0·12
Max. second-mode flutter amplitude, $\eta(1)_{max}$	0·15	0·08–0·10
Max. third-mode flutter amplitude, $\eta(1)_{max}$	0·11	0·08–0·10
Second-mode limit-cycle frequency (Hz^*)	2·5	~2·7
Third-mode limit-cycle frequency (Hz^*)	6·7	~6·7

Another discrepancy between theory and experiment is that in the latter a hysteresis has been observed in the onset of second-mode flutter; this has not been reproduced in the theory, the bifurcation always being supercritical.

Table 2 shows a comparison between the dimensionless amplitudes and the dimensionless limit-cycle flutter frequencies. It can be seen that the theoretical amplitudes are larger than the experimental ones, but the frequencies, both for second- and third-mode flutter, are in good agreement. It should be noted that the amplitudes are more difficult to measure than the frequencies.

6. CONCLUSION

The dynamics of cantilevered slender cylinders in axial flow has been examined anew in this three-part study. In Part 1, the experimental observations are described, summarizing the results for some older experiments and those from a new experimental programme. Then, the mechanisms involved in the two principal modes via which the system loses stability, divergence and flutter, have been clarified. Based on the insights gained thereby, the theoretically predicted physical dynamics of the system, reasoned rather than calculated, was found to agree with that observed experimentally. Part 2 is entirely devoted to obtaining a nonlinear equation of motion via Hamilton's principle, sufficient for the study of weakly nonlinear motions.

In Part 3, this paper, the linearized and nonlinear versions[†] of the theoretical model are utilized to explore the bifurcational behaviour and nonlinear dynamics of the system.

In terms of linear dynamics, the main bifurcations arising, as the flow velocity is increased, are: divergence in the first mode, restabilization, but not always, and then second-mode flutter, followed by higher-mode divergence and flutter, sometimes concurrently.

The effect of some of the key parameters affecting these bifurcations were explored. The effect of the free-end shape was investigated first by varying the free-end slenderness parameter f and the associated base drag coefficient c_b (Figure 1). Then, the effect of varying f and also the transverse and longitudinal frictional coefficients εc_N and εc_T was looked into, in the latter case varying εc_N and c_N/c_T (Figures 3 and 4). It is clear from Figures 1, 3 and 4 that for optimum stability the free end should be blunt (f should be small) and εc_N should be large; in practice, meaning that $\varepsilon = L/D$ should be large, which may appear to be counter-intuitive. The effect of varying c_N/c_T alone is more intricate,

[†]Some calculations were conducted with the earlier, slightly different version of the nonlinear theory—different insofar as γ- and h-related terms are concerned (Appendix A of Part 2). Any effects on the results should be minimal, since $h = 0$ and $\gamma = 1{\cdot}9$, which is small (γ beginning to play a significant role if it is of order 10 or larger).

and it is discussed in Section 3.3. Finally, the effect of varying the mass ratio β was also explored. Although it does not have a dramatic effect on stability, β is nevertheless one of the key parameters controlling whether there is restabilization of the system prior to the onset of flutter.

The system was then examined from the nonlinear point of view, using the tools of nonlinear dynamics theory. One important result obtained is that post-divergence flutter *does* materialize [cf. Païdoussis (1998, Chapter 5) for the opposite result], whether there is post-divergence restabilization or not.

Then, the nonlinear dynamics was explored for one particular system, with parameters close to those of the experimental system. It is found that the cylinder first loses stability by divergence in its first mode, the amplitude of which increases with flow; this is gradually transformed to divergence of predominantly second-mode shape, before the system is restabilized—in most but not all cases. At slightly higher flow velocities, the system loses stability by second-mode flutter, which at still higher flows is succeeded by third-mode flutter. The transition between these two forms of flutter encompasses a zone of aperiodic or quasiperiodic motions. It is of special interest that multiple solutions may coexist in some parameter ranges, and they depend on initial conditions.

Both linear aspects (the critical flow velocities for the principal bifurcations) and nonlinear aspects (amplitudes, limit-cycle frequencies, transition between the various dynamical states, quasiperiodicity) are compared with experimental observations. Broadly, theory and experiment are in good qualitative and reasonably good quantitative agreement. The key bifurcations are predicted within 7–25%, while the amplitudes to $\sim$100% only, and the limit-cycle frequencies (surprisingly) to 7%. In this regard, it should be said that the theoretical behaviour, especially at higher flows was found to require a high number of Galerkin modes, in fact more than that could be comfortably accommodated in the numerical calculations. Yet, some aspects of observed behaviour (e.g., hysteresis) are not reproduced by theory.

It is concluded that the results obtained in this study lend confidence that the theoretical model is sound, even though improvements may be desirable.

In the theoretical model, as developed in Part 2, the flexible slender body is considered to consist of (i) a long, uniform cylindrical part, and (ii) a short tapering end-piece attached to the free end thereof, with these two components being treated separately and somewhat differently. As pointed out by one of the referees, with whom we agree, it would be interesting to redo the theoretical model, treating the system as a single flexible body of nonuniform cross-section, by means of classical slender-body theory [see, e.g., Bisplinghoff *et al.* (1955), Dowell *et al.* (1995), Païdoussis (2002, Chapter 8)]. This model could be used to obtain predictions which would then be compared with the statements made on energy transfer mechanisms (Part 1), where the tapering end has been shown to play an important rôle. The viscous terms could then be incorporated into the model in a similar manner as done in Part 2. Work in this direction is underway.

ACKNOWLEDGEMENTS

The authors gratefully acknowledge the support received from the Natural Sciences and Engineering Research Council of Canada and Le Fonds FCAR of Québec.

REFERENCES

AUGU, N. 1999 Nonlinear dynamics of a cylinder subjected to an axial external flow. DEA Report, Département de Mécanique, École Centrale de Nantes, France.

Bisplinghoff, R. L., Ashley, H. & Halfman, R. L. 1955 *Aeroelasticity*, p. 418 *et seq*. Reading, MA: Addison-Wesley.

Doedel & Kernéves 1986 AUTO: software for continuation and bifurcation problems in ordinary differential equations. Applied Mathematics Report, California Institute of Technology, Pasadena, California, U.S.A. (obtainable from doedel@cs.concordia.ca).

Dowell, E. H., Crawley, E. F., Curtiss, H. C. Jr, Peters, D. A., Scanlan, R. H. & Sisto, F. 1995 *A Modern Course in Aeroelasticity*, 3rd edition, p. 99 *et seq*. Dordrecht: Kluwer Academic Publishers.

Lopes, J. L., Païdoussis, M. P. & Semler, C. 1999 Nonlinear dynamics of a cylinder in steady axial flow. MERL Report 99–2, Mechanical Engineering Research Laboratories, Department of Mechanical Engineering, McGill University, Montreal, QC, Canada (MERL Reports are available in digital form from www.library.mcgill.ca/psel/subguide/mecheng.htm).

Lopes, J. L., Païdoussis, M. P. & Semler, C. 2002 Linear and nonlinear dynamics of cantilevered cylinders in axial flow. Part 2: the equations of motion. *Journal of Fluids and Structures* **16,** 715–737.

Moon, F. C. 1992 *Chaotic and Fractal Dynamics*. New York: John Wiley.

Païdoussis, M. P. 1998 *Fluid–Structure Interactions: Slender Structures and Axial Flow*. Vol. 1. London: Academic Press.

Païdoussis, M. P. 2002 *Fluid-Structure Interactions Slender Structures and Axial Flow*. Vol. 2. London: Academic Press.

Païdoussis, M. P., Lopes, J. L. & Semler, C. 1999 Nonlinear equations and dynamical behaviour of a cantilevered cylinder in axial flow. *Engineering Mechanics* **6,** 285–300.

Païdoussis, M. P., Grinevich, E., Adamovic, D. & Semler, C. 2002 Linear and nonlinear dynamics of cantilevered cylinders in axial flow. Part 1: physical dynamics. *Journal of Fluids and Structures* **16,** 691–713.

Païdoussis, M. P. & Semler, C. 1993*a* Nonlinear and chaotic oscillations of a constrained cantilevered pipe conveying fluid: a full nonlinear analysis. *Nonlinear Dynamics* **4,** 655–670.

Païdoussis, M. P. & Semler, C. 1993*b* Nonlinear dynamics of a fluid-conveying cantilevered pipe with an intermediate spring support. *Journal of Fluids and Structures* **7,** 269–298.

Semler, C., Gentleman, W. C. & Païdoussis, M. P. 1996 Numerical solutions of second-order implicit ordinary differential equations. *Journal of Sound and Vibration* **195,** 553–574.